RSC Advances

PAPER

Cite this: *RSC Adv.*, 2024, **14**, 11872

Benzoic acid inhibits intrinsic ion migration for efficient and stable perovskite solar cells

Lijun Su, * Xiaoran Chen, Xinyu Wu and Jing Pan

Received 23rd January 2024
Accepted 2nd April 2024

DOI: 10.1039/d4ra00583j

rsc.li/rsc-advances

An efficient perovskite solar cell (PSC) has the following characteristics: (1) large perovskite grain size; (2) small ion migration; (3) low defect density states. Here, benzoic acid was employed as an additive to a perovskite solution to improve the thin film quality. Surprisingly, 1.0%-BA can implement all of these features. Therefore, the power conversion efficiency (PCE) of the champion PSC is 18.05%, which is superior to that of the control device (15.42%). In addition, BA-doped PSC kept 86% of its primary PCE after 30 days (RH: 35%), but the control device only retained 75% under the same conditions. The improvement of its stability is because of the inhibition of the cation migration of perovskite by the addition of BA and the passivation of perovskite defects. The results can acquire a better understanding of the potential applications of small organic molecules in improving the PCE and stability of PSC devices.

1 Introduction

Owing to the low cost of materials, high efficiency and easy preparation processability, perovskite solar cells (PSCs) have attracted considerable attention in the field of photovoltaics.[1–3] Nowadays, PSC has realized a power conversion efficiency (PCE) of 26.1%, comparable with those of the market silicon solar cells, which is mainly attributed to the low excitation energy, excellent light absorbency and long carrier lifetime of halide perovskite materials.[4–9] Although the PSC has made some progress in recent years, the defects of grain boundary, I vacancy (V_I) and Pb vacancy (V_{PB}) in hybrid perovskite films are still striking.[1,3,10] The above defects and the grain boundaries can be named as trap states, trapping/recombining photogenerated carriers,[11–14] which severely affects the PSC efficiency and device stability.[15–18]

The grain boundary is an important part of the trap state, a channel for ion migration and the specific location of water-etched perovskite. Therefore, it is very important to prepare high quality perovskite films with a larger grain size and smaller grain boundary to reduce trap state density, inhibit ion migration and reduce external water and oxygen erosion. There are many defects in a perovskite besides grain boundary. These not only cause non-radiative recombination of photocarriers, but also adsorb water and oxygen molecules from the air, thus reducing the efficiency and stability of the devices.

Some efforts have been made to passivate or eliminate these defects.[19] At present, the two-step solution method is regarded as an effective method for preparing perovskite films, which has a controllable morphology and better reproducibility than the one-step solution method. In addition, additive engineering has been proved to be another way to solve these defects.[20–24] The universally used passivators include inorganic metal salts,[25,26] organic small molecules,[27] and polymers.[28] There are some passivators, including carbonyls and the benzene ring, which are rich in electron functional groups, that can bind to uncoordinated Pb^{2+} ions/halide anions in the perovskite,[20,23] thus effectively reducing deep-level defects. In addition, uncoordinated Pb^{2+} ions are more sensitive to moisture than to halogen anions.[29,30] Therefore, it is urgent to use an effective passivation strategy to eliminate the uncoordinated Pb^{2+} ions. 3,5-Bis(trifluoromethyl)benzoic acid was used as an additive in $(FAPbI_3)_{0.85}(MAPbBr_3)_{0.15}$ to suppress trap-assisted nonradiative recombination.[31] Bark *et al.* employed trimesic acid in a PSC to reduce carrier recombination.[32] Mishra *et al.* used BA post-treatment in $CsPbBr_3$ PNCs to improve the PL and long-term stability.[33] However, there are few reports on the improvement of PSC performance by an additive two-step method.

For the above research situation, a benzoic acid (BA) additive was introduced into the perovskite precursor solution to creatively prepare high quality films. BA has many functions: (1) to stabilize the composition of the perovskite and inhibit the internal ion migration; (2) to induce the growth of large perovskite grains, reduce the defects and inhibit the erosion of the perovskite by water and oxygen. Ultimately, the efficiency and stability of the PSCs are greatly enhanced.

2 Experimental section

2.1 Materials and reagents

FTO glass, $Ti(iPrO)_2(acac)_2$ and spiro-OMeTAD were ordered from LumTec. Lithium bis-(trifluoromethylsulfonyl)imide

Department of Materials and Chemical Engineering, Taiyuan University, Taiyuan, 030032, P. R. China. E-mail: lijunsu@126.com

(>99.95%), CH_3NH_3I (MAI), lead iodide, $TiCl_4$, and benzoic acid (BA, 99%, $M_w = 122.12$ g mol^{-1}) were provided from Aldrich.

2.2 Device fabrication

Distilled water and isopropanol were used to clean the FTO glass, sequentially. The FTO was dried with a N_2 stream and treated with UV ozone for 20 minutes. The compact TiO_2 was spin-coated at 2000 rpm, 1000 rpm s^{-1} for 35 s using $Ti(iPrO)_2(acac)_2$ (0.3 M) in 2-propanol, which was heated at 125 °C for 10 minutes and 450 °C for 40 minutes. After the substrates cooled down, the $TiCl_4$ solution was used to immerse the substrates at 70 °C for 25 minutes. The mesoporous TiO_2 (30 nm particle size) layer was prepared with 5000 rpm for 40 s, then annealed at 125 °C for 10 minutes and 450 °C for 40 minutes.

$MAPbI_3$ was deposited in a glovebox by a two-step deposition. First, PbI_2 solution (1 M) was made by dissolving in DMF : DMSO (7 : 3 volume ratio). Then, 60 μL of the solution was spun at 5000 rpm for 60 s. Subsequently, the MAI (dissolved in IPA) without or with different amounts (0.5, 1.0, and 1.5%, mass ratio of BA *vs.* MAI) of BA was spun onto the PbI_2 film at 4000 rpm for 30 s and annealed at 120 °C for 45 minutes. Also, 40 μL of a spiro-OMeTAD (60 mM) solution was dropped at 2000 rpm for 35 s on $MAPbI_3$, where 30 mM Li-TFSI and 200 mM 4-*tert*-butyl-pyridine was added in spiro-OMeTAD. Finally, 100 nm of Au was evaporated to complete the device fabrication.

2.3 Measurements and characterization

The UV-Vis measurements were done using a Cary 60 UV-Vis Spectrophotometer. The XRD patterns were obtained to describe the crystalline structure of the perovskite films by an XRD Rigaku DMAX 2200. FTIR spectra were recorded by a Vertex 7 infrared spectrometric analyzer. The cross-section and top-view images were done by FEI Quanta 600 microscopy. The steady-state PL was determined using an FLS980 spectrometer. The *J*–*V* was tested under 100 mW cm^{-2}, AM 1.5 (1 Sun conditions), using a Solar Simulator (ABET 11000). The size of the devices was 0.09 cm^2. The EQE was measured under wavelengths from 300 nm to 900 nm.

3 Results and discussion

To study the effect of BA additive on the morphology of the perovskite, SEM was conducted. With the increase of BA content from 0 to 1.0%, the grain size of $MAPbI_3$ becomes larger (Fig. 1a–c). While if the BA content is further increased to above 1.5%, a perovskite film with many pinholes can be observed (Fig. 1d). Moreover, the grain size of the perovskite improved with the increase of BA amount. However, the 1.5%-BA film showed poor quality, which was attributed to the agglomeration of excess BA in the $MAPbI_3$ film. This result indicates that the BA additive could affect the growth manner of the $MAPbI_3$ film. In detail, delayed crystallization is an effective way to control the crystallization process to obtain high quality perovskite films. After adding quantitative BA into MAI, the BA, which has a carboxyl group and a benzene, has a strong interaction with Pb^{2+} by a chelation effect to form an intermediate phase. The intermediate phase turned into the perovskite phase with the removal of solvents during the heating process and prolonged the crystallization time. As the reaction progresses, the BA could crosslink adjacent perovskite grains, which promoted the interconnectivity of the film and obtained the large grain size film. However, when an excess amount of BA was added, the excess intermediate phase might in turn hinder the formation of perovskite films, resulting in a poor perovskite film quality with many small particles. The cross-sectional SEM image of a PSC based on a bare perovskite film with an advantageous thickness of 400 nm is shown in Fig. 1e, ensuring adequate light absorption due to a reduced recombination.

The BA additive effect on the perovskite crystallinity was measured using XRD. XRD spectra of the photoactive film without and with 1.0% BA additive are shown in Fig. 1f. The peaks at 2θ of 14.11, 19.91, 23.28, 24.47, 28.15 and 42.86 can be indexed to the (1 1 0), (1 1 2), (2 1 1), (2 0 2), (2 2 0) and (3 1 4) of the perovskite film, respectively. The peaks at 26.45 and 37.69 might belong to the FTO glass. No new peak appears or a clear peak shift after BA passivation, implying BA did not influence the perovskite lattice. The typical diffraction peaks at 14.11° can be indexed to the (1 1 0) plane of BA-perovskite grains which is stronger than that of pristine $MAPbI_3$, indicating that the BA additive can improve the crystallinity of the perovskite. The peak at 12.32° in the $MAPbI_3$ films and $MAPbI_3$ with 1.0% BA additive may be due to the incomplete reaction between MAI and PbI_2.

Fig. 2 analyzes the interactions between BA and perovskite using Fourier transform infrared (FTIR) spectra. The C=O vibration band of BA in the photoactive film shifted from 1687 to 1631 cm^{-1}, indicating that the –COOH group in perovskite films formed a chemical bond with Pb ions (Scheme 1).[32]

The UV-Vis absorption spectra of the $MAPbI_3$ film are presented in Fig. 3A without and with different amounts of BA additive. With the increase of BA amount from 0 to 1.0%, the optical absorption strength of the perovskite films increases gradually, which is due to the increase of crystallinity and perovskite grain size. However, the light absorption of the 1.5% BA-doped perovskite film decreased because of the large amount of small perovskite grains. For Fig. 3B, the intensity of PL increased significantly for the $MAPbI_3$ film with 1.0%-BA in comparison to the bare $MAPbI_3$ film, which may be ascribed to

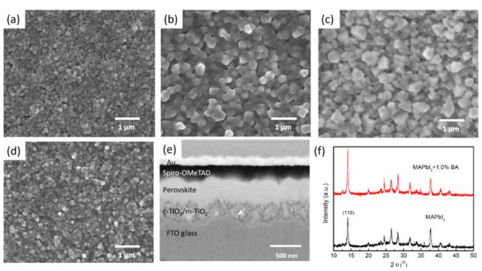

Fig. 1 (a)–(d) Top-view SEM images of $MAPbI_3$, 0.5, 1.0, and 1.5% BA additive films. (e) Cross-sectional SEM image of the $MAPbI_3$ films, (f) XRD patterns of the $MAPbI_3$ films and $MAPbI_3$ with 1.0% BA additive, respectively.

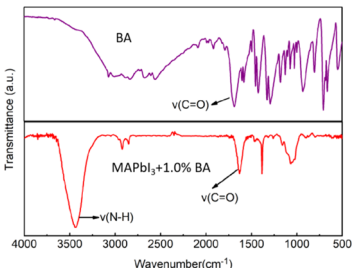

Fig. 2 FTIR spectra of BA and $MAPbI_3$ + 1.0% BA, respectively.

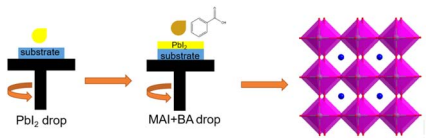

Scheme 1 Diagram of perovskite and BA.

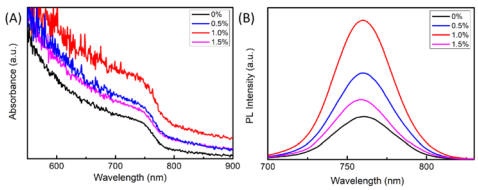

Fig. 3 (A) UV-Vis absorption and (B) steady-PL spectra of PSCs based on Fig. 1(a)–(d) 0, 0.5, 1.0, and 1.5% BA additive films, respectively.

Table 1 The photovoltaic parameters of the champion PSCs based on the *J*–*V* curves in Fig. 4

PSC	J_{SC} (mA cm^{-2})	V_{OC} (V)	FF	PCE (%)
a	21.71	1.03	0.69	15.42
b	22.72	1.06	0.71	17.10
c	23.00	1.09	0.72	18.05
d	22.79	1.03	0.71	16.66

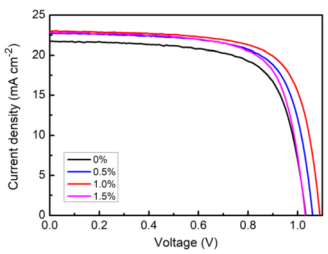

Fig. 4 *J*–*V* curves of PSCs based on 0, 0.5, 1.0, and 1.5% BA additive-$MAPbI_3$ films, respectively.

the passivation effect of BA. This could be due to a high-quality crystallinity and fewer defects of the $MAPbI_3$ with BA.

To further investigate the effect of BA on the photovoltaic performance of the PSC, *J*–*V* curves were tested. The perovskite film containing 1.0% BA additives showed a champion PCE = 18.05%, V_{OC} = 1.09 V, J_{SC} = 23.00 mA cm^{-2}, and FF = 0.72, indicating an optimal BA content of 1.0% (Table 1 and Fig. 4). The improvement in PSC efficiency due to the increased V_{OC} and J_{SC} can be attributed to the improved optical properties and good quality of the photoactive films (Table 1). With the increase of BA content to 1.5%, the PCE decreased to 16.66%, which may be due to the formation of rough perovskite films with multiple pinholes (Fig. 5).

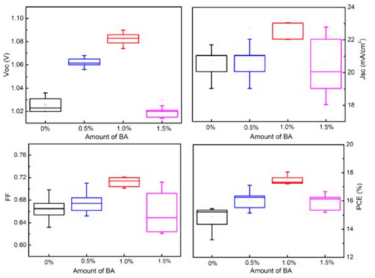

Fig. 5 Statistics for the different parameters of the measured solar cells (20 samples) for 0, 0.5, 1.0, and 1.5% BA additive-$MAPbI_3$ films, respectively. It presents the distribution of device parameters. It can be observed that the *J*sc increases obviously for the 1.0%-BA PSC. The enhancement of the *J*sc can be attributed to the improved film quality. Moreover, the statistics of the parameters show a narrow distribution for 1.0% BA-$MAPbI_3$, which indicates the great reproducibility of the devices.

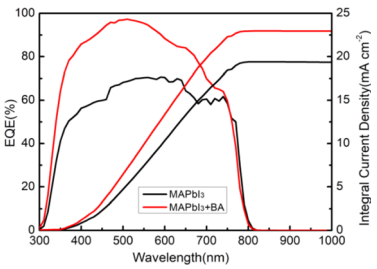

Fig. 6 EQE spectra and integrated current density of $MAPbI_3$ and $MAPbI_3$ + 1.0% BA.

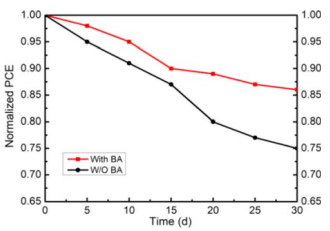

Fig. 7 Normalized PCE values of PSCs *versus* aging time (room temperature, RH: 35%, time: 30 days).

Fig. 6 shows the EQE spectra of PSCs with BA in contrast to that of the bare cell. The light response from the EQE spectra was significantly increased in the wavelength range of 300–800 nm and the BA-doped PSC was approximately 80%. This could be attributed to the enhanced film quality, as shown in the SEM images. The integrated current densities for the $MAPbI_3$ and $MAPbI_3$ + 1.0% BA devices were calculated to be

19.2 and 22.7 mA cm^{-2}, respectively, matching the *J*sc measured from the *J*–*V* curve.

Apart from the efficient photovoltaic performance, we also explored the humidity stability. The time evolutions of PCE for PSCs without and with BA are shown in Fig. 7. The unencapsulated devices were stored in ambient air with a RH of 35%. The PSCs with a BA additive maintained over 86% of the original PCE after 30 days, *versus* pristine PSCs, which only retained 75% under the same conditions. The BA improves the stability of the composition due to the structure of BA, which has a carboxyl group and a benzene ring. The hydrogen bond (hydroxyl group and iodide) suppresses the migration of iodine ions, preventing the perovskite from decomposing. Also, the benzene ring as the hydrophobic alkyl chain could prevent the reaction of the perovskite with water.

4 Conclusions

To sum up, we introduce a multifunctional BA molecule into an $MAPbI_3$ film to passivate the defect. BA with a –COOH group can bind to uncoordinated Pb^{2+} and I^- ions, reducing the defect density and inhibiting the internal ion migration. The PCE of a BA-doped PSC was 18.05%, which is higher than that of the control device. Moreover, the BA passivated devices showed an improved device stability. After being stored in ambient air for 30 days (temperature: 25 °C and RH: 35%), the unencapsulated devices retained 86% of the initial PCE, *versus* the PCE of the control device at only about 75%.

Author contributions

All the authors contributed to the study conception and design. Lijun Su: supervision, resources, funding acquisition, project administration, writing review and editing; Xinyu Wu and Xiaoran Chen: methodology, materials preparation, data collection and analysis investigation. All authors commented on previous versions of the manuscript. All authors read and approved the final manuscript.

Conflicts of interest

There are no conflicts to declare.

Acknowledgements

This work was financially supported by the Fund for the Nature Science Foundation of Shanxi Province, China (Grant No. 202203021222414), Shanxi Scholarship Council of China (2022-183), the Higher Education Science and Technology Innovation Program of Shanxi Province, China (Grant No. 2022L584), and the Innovation and Entrepreneurship Program for College Students of Shanxi Province (TYX2023023, TYX2023083).

References

1 Y. Wu, H. Zhu, B. B. Yu, S. Akin, Y. Liu, Z. Shen, L. Pan and H. Cai, *Chem. Eng. J.*, 2022, **433**, 134613.
2 Y. Zhang, L. Xu, Y. Wu, Q. Zhou, Z. Shi, X. Zhuang, B. Liu, B. Dong, X. Bai, W. Xu, D. Zhou and H. Song, *Nano Energy*, 2021, **90**, 106610.
3 S. Zhu, J. Wu, W. Sun, W. Pan, F. Cai, J. Liu, L. Chen, X. Chen, C. Wang and X. Wang, *ACS Appl. Energy Mater.*, 2022, **5**, 658–666.
4 C. Chen, S. Zheng and H. Song, *Chem. Soc. Rev.*, 2021, **50**, 7250–7329.
5 National Renewable Energy Laboratory, *Best Research-Cell Efficiencies*, 2024, **http://www.nrel.gov/pv/cell-efficiency.html**.
6 B. Boro, S. Porwal, D. Kumar, S. Mishra, S. Ghosh, S. Kansal, A. Chandra and T. Singh, *Catal. Res.*, 2022, **2**, 1–48.
7 M. L. Sun, C. X. Zhao, J. F. Shu and X. Yin, *Funct. Nanomater.*, 2022, 225273.
8 H. Xi, Z. Song, Y. Guo, W. Zhu, L. Ding, W. Zhu, D. Chen and C. Zhang, *Polymers*, 2022, **14**, 2748.
9 R. Kottayi, D. K. Maurya, R. Sittaramane and S. Angaiah, *ES Energy Environ.*, 2022, **18**, 1–40.
10 Y. Zhang and N. G. Park, *ACS Energy Lett.*, 2022, **7**, 757–765.
11 S. Ma, G. Yuan, Y. Zhang, N. Yang, Y. Li and Q. Chen, *Energy Environ. Sci.*, 2022, **15**, 13–55.
12 J. E. Kim, S. S. Kim, C. Zuo, M. Gao, D. Vak and D. Y. Kim, *Adv. Funct. Mater.*, 2019, **29**, 1809194.
13 Y. Zhang, Y. Li, L. Zhang, H. Hu, Z. Tang, B. Xu and N. G. Park, *Adv. Energy Mater.*, 2021, **11**, 2102538.
14 S. Xiong, Z. Hou, W. Dong, D. Li, J. Yang, R. Bai, Y. Wu, D. Li, H. Wu, Z. Ma, J. Xu, X. Liu and Q. Bao, *Adv. Energy Mater.*, 2021, **11**, 2101394.
15 D. D. Girolamo, N. Phung, F. U. Kosasih, F. D. Giacomo, F. Matteocci, J. A. Smith, M. A. Flatken, H. Kobler, S. H. T. Cruz, A. Mattoni, L. Cina, B. Rech, A. Latini, G. Divitini, C. Ducati, A. D. Carlo, D. Dini and A. Abate, *Adv. Energy Mater.*, 2020, **10**, 2000310.
16 L. Duan and A. Uddin, *Mater. Chem. Front.*, 2022, **6**, 400–417.
17 R. Xia, X. X. Gao, Y. Zhang, N. Drigo, V. I. E. Queloz, F. F. Tirani, R. Scopelliti, Z. Huang, X. Fang, S. Kinge, Z. Fei, C. Roldan-Carmona, M. K. Nazeeruddin and P. J. Dyson, *Adv. Mater.*, 2020, **32**, 2003801.
18 W. Yang, D. Zhong, M. Shi, S. Qu and H. Chen, *Science*, 2019, **22**, 534–543.
19 F. Gao, Y. Zhao, X. Zhang and J. You, *Adv. Energy Mater.*, 2020, **10**, 1902650.
20 G. Tong, L. K. Ono and Y. Qi, *Energy Technol.*, 2020, **8**, 1900961.
21 T. Wu, Z. Qin, Y. Wang, Y. Wu, W. Chen, S. Zhang, M. Cai, S. Dai, J. Zhang, J. Liu, Z. Zhou, X. Liu, H. Segawa, H. Tan, Q. Tang, J. Fang, Y. Li, L. Ding, Z. Ning, Y. Qi, Y. Zhang and L. Han, *Nano-Micro Lett.*, 2021, **13**, 152–169.
22 Y. Ahmed, B. Khan, M. Bilal Faheem, K. Huang, Y. Gao and J. Yang, *J. Energy Chem.*, 2022, **67**, 361–390.
23 D. Xin, S. Tie, X. Zheng, J. Zhu and W. H. Zhang, *J. Energy Chem.*, 2020, **46**, 173–177.
24 S. Yun, S. Ma, H. Kwon, K. Kim, G. Jang, H. Yang and J. Moon, *Nano Energy*, 2019, **59**, 481–491.

25 T. Bu, J. Li, F. Zheng, W. Chen, X. Wen, Z. Ku, Y. Peng, J. Zhong, Y.-B. Cheng and F. Huang, *Nat. Commun.*, 2018, **9**, 4609.
26 S. Yang, S. Chen, E. Mosconi, Y. Fang, X. Xiao, C. Wang, Y. Zhou, Z. Yu, J. Zhao and Y. Gao, *Science*, 2019, **365**, 473–478.
27 J. Yang, W. Tang, R. Yuan, Y. Chen, J. Wang, Y. Wu, W. J. Yin, N. Yuan, J. Ding and W. H. Zhang, *Chem. Sci.*, 2021, **12**, 2050–2059.
28 Q. Wang, Q. Dong, T. Li, A. Gruverman and J. Huang, *Adv. Mater.*, 2016, **28**, 6734–6739.
29 M. Thambidurai, B. Febriansyah, S. Foo, P. C. Harikesh, K. T. Ming, N. Mathews and C. Dang, *J. Power Sources*, 2020, **479**, 228811.
30 H. Si, C. Xu, Y. Ou, G. Zhang, W. Fan, Z. Xiong, A. Kausar, Q. Liao, Z. Zhang, A. Sattar, Z. Kang and Y. Zhang, *Nano Energy*, 2020, **68**, 104320.
31 X. D. Ding, H. X. Wang, Y. W. Miao, C. Chen, M. D. Zhai, C. S. Yang, B. Y. Wang, Y. Tian and M. Cheng, *ACS Appl. Mater. Interfaces*, 2022, **14**, 3930–3938.
32 H. V. Quy, D. H. Truyen, S. Kim and C. W. Bark, *ACS Omega*, 2021, **6**, 16151–16158.
33 V. G. Dutt, S. Akhil, R. Singh, M. Palabathuni and N. Mishra, *J. Phys. Chem. C*, 2022, **126**, 9502–9508.